Multiscale Layered Biomechanical Model of Pacinian Corpuscle

Abhijit Biswas, M. Manivannan and Mandayam A. Srinivasan

Abstract—This paper describes a multiscale analytical model of lamellar-structure and biomechanical response of Pacinian Corpuscle (PC). In order to analyze the contribution of the PC lamellar-structure for detecting high frequency vibrotactile (VT) stimuli, covering few 10s of Hz to few kHz, the model response is studied against trapezoidal and sinusoidal stimuli. The model proposes few generalizable features of PC lamellar-structure which makes it scalable for different sizes of PC with different number of lamella. The model describes mechanical signal conditioning of lamellar-structure in terms of a recursive transfer-function, termed as Compression-Transmittance-Transfer-Function (CTTF). The analytical results show that with the increase of the PC layer index above 15, the PC inner core relaxes within 1 ms against step-compression applied to the outermost layer. This model also considers mass of each PC layer in order to investigate its effect on the high frequency biomechanical response of the lamellar-structure. The interlamellar spacing and its biomechanical properties along with the model response is validated with experimental literature. The proposed model can be used for simulating a network of PCs considering its diversity in terms of size, lamella-number and material properties for analyzing high-frequency VT sensitivity of human skin.

Index Terms—Lamellar structure, Viscoelastic property, Biomechanical response, Compression transmittance transfer function

1 Introduction

Pacinian Corpuscle (PC) is the largest mechano-receptor found in human body and widely distributed in skin, joints and viscera. After the first discovery of PC in 1741 by Lehmann, as reported in [1], the anatomical details of three major parts of PC: Nerve Fiber (NF), Inner Core (IC) or simply core and perineural capsule are reported as early as 1911 [2]. Although the last century witnessed more anatomical and histochemical detailing of PC upto sub-micrometer level, only a very few studies attempted to mathematically model its biomechanical properties [1], [3], [4]. These earlier models are not scalable considering the diversity in PCs. In order to develop a scalable and more accurate model of PC, first we have summarized the anatomical details of its lamellar structure [1], [2], [5] including recent discoveries [1], [6], [7], [8], [9], [10] that are not considered in [3]. Apart from the anatomical details, recent discoveries on histochemistry of PC [1], [6], [8] leads to the identification of few key features of the lamellar structure that can be used for developing a scalable model of PC. The major application of such model could be in characterization of vibrotactile sensitivity of skin and in understanding the physiology and pathology [11], [12] related to PC.

Biomechanical response of PC is first detailed in [4] experimentally and modeled in [3]. These two pioneering works indicate that the mechanism behind extreme sensitivity of PC towards the high frequency vibrotactile stimuli is the rapid biomechanical response (relaxation against steady indentation) of its inner core and axolemma of the nerve fiber. Such rapid adaptiveness of the PC core is mainly found to be the result of mechanical signal filtering performed by the lamellar structure inside the capsule [4]. Based on this experimental finding, Loewenstein and Skalak [3] have derived a first biomechanical model of the PC. Though the model response does not match the experimental results well [13], [14] and mass of the PC layers are also neglected, the theoretical analysis in [3] offers a valuable framework to build more accurate and generic model of PC. Another drawback of the model in [3] is that it treats the PC core as a rigid object. This assumption is a serious limitation restricting the integration of biomechanical and neurophysiological models, as a rigid object can not be stretched and the stretch activated ion channels in PC core membrane are critical for the mechanotransduction [9], [15].

The main objective of this paper is to analyze the effect of size variability of PC by developing a scalable layered biomechanical model of PC which can describe the experimental relaxation response [4] more accurately than that of [3]. Therefore first we have proposed a generalized relation between PC size and the number of lamella present in it. Though we have modeled the PC as concentric fluid filled cylinders similar to [3], it includes a more reasonable interlamellar spacing with viscoelastic core in it. Next we have considered the mass of each layer to investigate its effect on frequency response even beyond 1 kHz. More appropriate material properties are chosen in order to match the experimental results [4].

- *Abhijit Biswas and M. Manivannan are with the Touch Lab, Biomedical Research Group, Department of Applied Mechanics, IIT Madras, Chennai, India. Email: mani@iitm.ac.in*
- *Mandayam A. Srinivasan is with the Touch Lab, Department of Mechanical Engineering and the Research Laboratory of Electronics, MIT, Cambridge, MA, USA as well as the Touch Lab, Department of Computer Science, University College London, UK. Email: srini@mit.edu*

Manuscript submitted 6 Apr. 2014; revised 09 Aug. 2014

2 Model Description

2.1 Structural & material properties of PC layers

Perineural capsule : PC capsule (Fig. 1) may contain 20 to 70 squamous epithelial lamellae of <0.5 µm thickness and the interlamellar spaces are filled with viscous fluid containing scattered collagen fibrils [1], [6], [8], [10]. Typically each layer is separated by lamella which partly isolates the interlamellar fluid from the next layer [16]. The perineural capsule is typically segmented into three zones [1], [10] (Fig. 1) : growth zone (intermediate zone or innermost perineural lamellae), inner perineural lamellae (inner lamellae or outer core) and external capsule (outer lamellae). Few outer limiting lamellae of external capsule may also be considered as a separate zone [10]. These zones have different interlamellar spacing and compositions of extracellular matrix. However these zones are not always distinctly identifiable under microscope [10].

Inner core & neurite : PC inner core is constituted of closely spaced 25 to 50 layers of cytoplasmic extensions of specialized glia or Schwann cells. These cytoplasmic extensions are bilaterally wrapped around the oval axolemma [1], [2] of neurite having major and minor axis in the order of 6 and 12 µm [17]. The bodies of these glie are mainly found at the outer boundary of the inner core. The inner core (the outer most glia lamellae) is separated from the inner most perineural lamellae in growth zone by basal lamina and a narrow space (included in growth zone of Fig. 1) filled with amorphous matrix of collagen fibrils and fine filaments [6], [10].

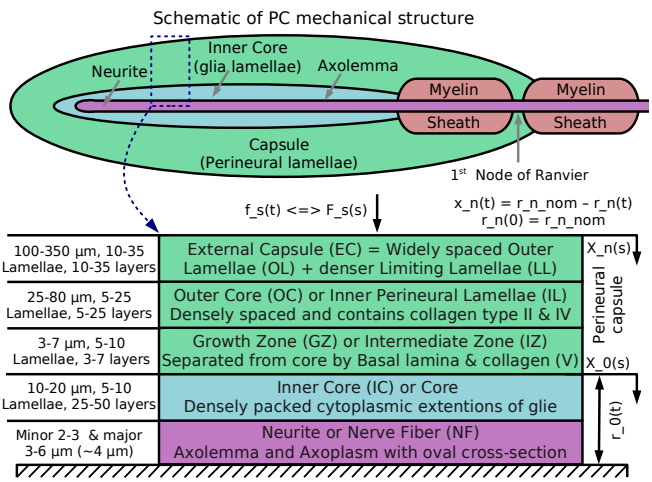

Fig. 1. Biomechanical model of PC lamellar structure (Lateral cross-section). The datum line represents the central axis of the neuron. The prefix '_' of the symbols in the figure indicates the subscripts as referred in following section. *f_s(t)* : force on outer most PC lamella, *F_s(s)* : Laplace transform of *f_s(t)*, *x_n(t)* : Compression over radius for nth PC layer, *X_n(s)* : Laplace transform of *x_n(t)*, *r_n_nom* : nominal radius of nth layer, *r_n(t)* : radius of nth layer at time *t*.

Heterogeneity of the capsule : PC capsule has inherent heterogeneity both in interlamella spacing and in the material properties of the interlamellar matrix. The innermost lamellae of growth zone (GZ) consist of densely packed multilamellar complex networked with collagen matrix derived from fibroblasts [6]. After GZ, the lamellae are spaced more than a few µm in the outer core and the spacing increases in the order of 10 µm at the periphery of external capsule after the outer core [8] (Fig. 1). However the outer most 5 to 7 lamellae of the external capsule are closely spaced and densely packed with collagen fibrils [6]. Throughout all the layers of the perineural capsule, the lamellae are attached with the basal lamina and extracellular matrix scattered with collagen fibrils.

2.2 Model parameters and approximations

PC is approximated as concentric cylinders filled with viscous fluid in each layer, which is similar to [3] with few major improvements. Each layer of the lamellar structure is modeled with four elements : two springs (parallel K_p and serial K_s), damper (B_s) and a mass (M) (Fig. 2). As PCs may have different numbers of lamella (Fig. 1), the developed model is parameterized with n (number of layer). The following parameters are used in the developed model.

n : Number of lamellae present in the PC capsule
i : Layer index ($0 \leqslant i \leqslant n$) and core is the 0th layer
m : Layer index ($1 \leqslant m \leqslant n$)
R_i : Nominal radius (*r_i_nom* in Fig. 1 and 2) of ith layer
E_{Li} : Elastic modulus of ith lamella
E_{Mi} : Elastic modulus for ith interlamellar matrix
U_i : Viscosity of fluidic part of ith interlamellar matrix
L : Length of the lamellae (1 mm for all layers)
T_i : Thickness of ith lamella
S_i : Thickness of ith interlamellar space
C_i : Cumulative thickness of ith interlamellar space
A_i : Radial surface area of ith layer
D_i : Density of ith layer

Approximations considered in the developed model are listed in the following section.

a) The term layer includes a lamella and interlamellar matrix adjacent to it. However occasionally more than one lamella jointly forms the layer separator in reality [16], which is treated as a single lamella for the purpose of modeling.
b) Interlayer material properties can be inhomogeneous but the intralayer material properties are homogenous.
c) Interlamellar fluid is viscoelastic and incompressible.
d) Although the fluid in PC capsule can move among the adjacent interlamellar space with a significant amount of resistance [5], this model assumes no leakage among the layers similar to [3]. In reality such isolation is mostly found in-between inner core and perineural capsule for the purpose of electrical isolation [1].
e) All other approximations such as approximation of shape of PC as concentric cylinder, equal length of all the layers and consideration of linear biomechanical model for individual layer as in [3] are equally applicable in this model.

2.3 Analytical relationship of model parameters

From Hubbard's experimental findings [4] it is possible to segment different zones of PC capsule either in terms of radii (1) or layer indices (2). The different zones in PC lamellar structure can be segregated in terms of limiting lamellae (LL), outer lamellae (OL), outer core (OC) and growth zone (GZ) (Fig. 1). Typically LL and OL can be combined as external capsule (EC). However Hubbard segmented the PC capsule into only two zones : external capsule (EC) and outer core (OC) considering the growth zone (GZ) as an integrated part of it. Following [1], [4] the radius of ith lamella of PC can be expressed as:

$$R_i = R_0 \gamma^i; \quad where\ \gamma = 1.1\ \forall\ R_i < 75\ \mu m; \ else\ \gamma = 1.08 \qquad (1)$$

For the PCs considered in [4], (1) can also be rewritten as (2) where R_0 = ~30 μm.

$$R_i = R_0 \gamma^i; \quad where\ \gamma = 1.1\ \forall\ i < 11\ ; \ else\ \gamma = 1.08 \qquad (2)$$

Combining (1 and 2) it is appropriate to consider first 10 to 15 outer core lamellae cover till 75 μm of PC radius. One of the limitations of (1 and 2) is that it does not consider the outer most 5 to 7 perineural lamellae which are closely spaced and densely packed with collagen fibrils [6]. Formulation of such relations (1 and 2) and generalizing over many variations of PCs is always a challenging task. One of such challenges is to measure the radius of PC lamella as it shrinks if punctured [2]. Therefore the lamellar clearance estimated from the microscopic slides, as reported in [1], [7], [8], [9], [10], may not be the exact functional interlamellar spacing.

From the theoretical analysis of [3] the value of the parallel spring (*K_p_i* in Fig. 2) representing the PC Lamellae can be determined by (3).

$$K_{pi} = \frac{E_{Li} A_i}{\frac{R_i^2}{T_i}\left\{1 + \frac{4L^2}{\pi^2 R_i^2}\right\}^2}; \quad \forall\, 0 < i \leqslant n \qquad (3)$$

The series spring and the damper (*K_s_i* and *B_s_i* in Fig. 2) representing the viscoelastic fluid in-between PC lamellae can be analytically expressed by (4 and 5).

$$K_{si} = \frac{E_{Mi} A_i}{R_i - R_{i-1} - T_i}; \ \forall\, 0 < i \leqslant n; \text{where } R_0 = \text{core-radius} \qquad (4)$$

$$B_{si} = \frac{12 U_i L^2 A_i}{\pi^2 (R_i - R_{i-1} - T_i)^3 \left\{1 + \frac{4L^2}{\pi^2 R_i^2}\right\}}; \quad \forall\, 0 < i \leqslant n \qquad (5)$$

2.4 Existing model Limitations & improvements

Although the PC is modeled as concentric fluid filled cylinders similar to [3], following list describes the major improvements in our model over the existing ones [3], [4].

a) PC lamellae thickness is found to be in the order of 0.09 to 0.4 μm [1], which is at least half the thickness of that considered in [3]. In our model the lamellae thickness increases following Weibull Function (6).

$$T_i = T_{mn} + (T_{mx} - T_{mn})\left(1 - \exp\left(-\left(\frac{i}{\alpha}\right)^{\beta}\right)\right); \forall\, 0 < i \leqslant n \text{ where} \qquad (6)$$
$$\alpha = n \times 90\,\%,\ \beta = 2.5,\ T_{mn} = 0.1\,\mu m \text{ and } T_{mx} = 0.4\,\mu m$$

b) PC core is modeled as a viscoelastic layer instead of a rigid object as in [3], because [9], [15], [18], [19] show that the neural activity of PC is controlled by strain or stretch sensitive ion-channels due to the deformation of the core. The entire core along with the nerve fiber is considered as a single layer for the purpose of modeling as the PC core is densely packed with glia lamellae and collagen within a radius of few 10s of μm (Fig. 1). We have assumed that a fraction of the overall core compression ($x_0(t)$) will represent the stretch signal applied on the stretch sensitive axolemma of PC.

c) The elastic modulus of PC lamellae as described in [3] is modified considering recent discoveries related to PC. Loewenstein and Skalak [3] assumed that the elastic modulus is same as that of the blood vessels. They considered elastic modulus = 0.5 MPa which is in the range of peak elastic modulus of blood vessels, moreover collagen fibers, one of the constituents of blood vessel, can offer even much higher elastic modulus (in the order of 100 MPa) [20], [21]. However we have considered the elastic modulus in the order of 1 kPa due to the following reason. Histochemical and anatomical literature [2], [6], [10] show that all the PC lamellae in the perineural capsule are attached with basal lamina from both sides which is mainly consisting of flexible type-IV basement-membrane-collagen and laminin [6], [8], [10], [22]. On the other hand, wall of the blood vessels has mainly type I & III collagen and elastin matrix [23], [24], providing better structural strength. This indicates that the lamellae elastic modulus should be in the order of stiffness of individual cell, closer to 1 kPa [1], [25], [26], which is definitely softer than that of the blood vessel wall. An attempt of directly measuring the elastic modulus of PC has shown that its elastic modulus is in the order of 1 kPa [1], rather than 0.5 MPa.

d) In [3] the viscosity of the PC interlamellar fluid is considered same as that of water which is also an over approximation, as it has a significant concentration of collagen which can be more than 1000 times viscous compared to water [27]. However water being the major constituent of interlamellar fluid (~92% [1]), the viscosity of the fluid is assumed to be higher but comparable with that of the water (0.7 mPa.s at human body temperature). Therefore a better choice of U_i could be 2 to 10 times than that of water.

e) Elastic component of the viscoelastic interlamellar matrix of PC is the most influential parameter governing the response of PC, which probably the most uncertain parameter in [3]. All the layers of the PC model in [3] have the same elastic modulus for the matrix which is 10^4 times less than that of the lamellae (E_{Li} : $E_{Mi} = 10^4$). Considering the recent literature [6], [10] it is clear that apart from the flexible type IV collagen, interlamellar spaces in PC capsule are filled with a fluid containing scattered collagen fibrils of type-II, and

type-V collagen is also found in the intermediate zone of perineural capsule [8]. Even the limiting interlamellar spaces of the capsule are densely packed with collagen [6]. Apart from collagen fibrils elastic fibers are also found scattered in the interlamellar matrix [6]. As collagen may be 1000s of times stiffer [20], [21] than individual cell stiffness [1], [25], [26], the elasticity of interlamellar matrix is governed by the type and density of collagen and elastic fibrils in it. Therefore we have chosen E_{Mi} of (4) in the range of 1 Pa ($E_{Li} : E_{Mi} = 10^3$).

f) According to Hubbard's relation (1 and 2) the thickness of ith interlamellar space (S_i) increases monotonically, which is found to be valid only for a small part of the PC capsule, whereas S_i found to be reducing (non-monotonic) towards the limiting lamellae (LL) of the capsule [1], [6], [10]. Probably for this reason Loewenstein and Skalak [3] could not simulate a PC with more than 30 layers, as the relation with 50 lamellae would result in an external diameter 2.5 mm which is impractical. While measuring the radius of LL, Hubbard might have grouped few of them together as they remain densely packed with collagen [6], [10]. Similarly the relation (1 and 2) does not take care of the growth zone of PC capsule, as it indicates the $S_i > 1$ µm even in the growth zone and outer core, which contradicts [16] and many other microscopic view of PC cross-sections [1], [6], [9], [10]. In order to generalize and improve the accuracy of the analytical relation between i and R_i we have followed a relativistic relation considering n number of layers present in PC capsule, where each zone contains certain percentage of n lamellae (starting from outermost layer of PC first 10% layers are LL, next 50% are Outer Lamellae (OL), next 30% are Outer Core (OC) and next 10% are Growth Zone (GZ)). Finding the exact value of n for a given PC is difficult compared to finding the R_n which itself is challenging as R_n shrinks if the capsule is punctured [2]. The relation among R_i, S_i, T_i and C_i are summarized in (7), where the parameter γ remains close to 1.3. The $\hat{R}_n$ (approximate value of R_n) can be directly measured under microscope which could be 150 to 450 µm [1], [4], [5]. On the other hand R_0 (typically 10 to 20 µm) can be measured from the sectional view of PC, has its definitive boundary [1] which is less altered against the external forces and preparation of microscopic slide.

$$S_i = (R_i - R_{i-1}) - T_i; \qquad \forall\ 0<i\leqslant n$$

$$R_i = R_0 + (\gamma\,\hat{R}_n - R_0) * \left(1 - \exp\left(-\left(\frac{i}{\alpha}\right)^{\beta}\right)\right) + i\,\delta; \quad \text{where} \qquad (7)$$

$$\alpha = n \times 90\%,\ \beta = 2.5,\ \gamma = 1.3 \text{ and } \delta = 0.5\,\mu m$$

g) In literature the mass of the lamellar structure is neglected. The mass of each PC layer in this model is included in order to investigate its effect in transmission of mechanical stimulus. For estimating the mass of each layer, we have chosen the density of all layers close to water (1000 to 1100 kg/m^3).

2.5 CTTF from PC outer layer to PC core

For modeling the mechanical signal transformation in PC lamellar structure, we have introduced a dimensionless parameter Compression Transmittance Transfer Function (CTTF $N_{pm}(s)$) relating the compression of the PC core (0th layer) as output, to the compression of the mth PC layer as input. The CTTF $N_{pm}(s)$ (for m=n) acts as a specialized high-pass filter for the mechanical compression at PC outermost layer ($x_n(t)$ in Fig. 2).

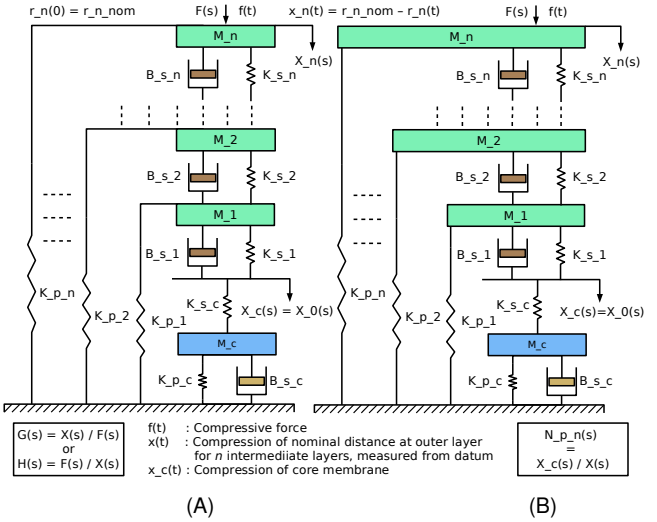

Fig. 2. Two possible equivalent biomechanical models of the PC based on relative arrangement of *K_p* and *M*. The prefix '_' of the symbols in the figure indicates the subscripts as referred in following section. *K_p* : Stiffness of parallel spring (representing lamella), *K_s* : Stiffness of serial spring (representing the elastic part of interlamellar matrix), *B_s* : Viscous frictional coefficient of the serial damper (representing the fluidic part of interlamellar matrix), *M* : mass of each layer.

Based on the relative arrangement of parallel spring (K_{pi}) and mass (M_i) two equivalent models of PC lamellar structure can be constructed (Fig. 2 A & B). If mass is neglected and the core is considered as rigid, both of these models will be reduced to the model described in [3]. In our earlier model [28] we had considered PC core layer (i=0) as Kelvin's viscoelastic model with mass which yields a strictly-proper 3rd order complex compliance (8). In this paper we preferred to model PC core (Fig. 2) by Voigt's model (K_{pc}, B_{sc}) with mass (M_c) and a serial spring (K_{sc}), as it represents a bi-proper 2nd order complex-compliance (9) which is more appropriate to model viscoelastic solids like soft tissue [29]. It is worth noting that another version of Kelvin's standard viscoelastic model with mass can also represent a bi-proper 2nd order complex-compliance which is not described in this paper [30].

$$G_0(s) = \frac{1}{H_0(s)} = \frac{X_0(s)}{F_0(s)} = \frac{1}{M_c s^2 + K_{pc} + \dfrac{1}{\dfrac{1}{B_{sc} s} + \dfrac{1}{K_{sc}}}} \qquad (8)$$

$$G_0(s) = \frac{1}{H_0(s)} = \frac{X_0(s)}{F_0(s)} = \frac{1}{M_c s^2 + B_{sc} s + K_{pc}} + \frac{1}{K_{sc}} \qquad (9)$$

Using the term $H_0(s)$ of (9), $H_1(s)$ for each model A & B (Fig. 2) are given in (10) and (11) respectively.

$$H_1(s)=\frac{1}{G_1(s)}=K_{p1}+\frac{1}{\frac{1}{M_1 s^2+B_{s1} s+K_{s1}}+\frac{1}{H_0(s)}} \quad (10)$$

$$H_1(s)=\frac{1}{G_1(s)}=M_1 s^2+K_{p1}+\frac{1}{\frac{1}{B_{s1} s+K_{s1}}+\frac{1}{H_0(s)}} \quad (11)$$

For ease of computation, we have considered model-A of Fig. 2 and (10) for further analysis and recursively derived the CTTF $N_{pm}(s)$, relating the compression of the nth layer ($x_n(t)$) to the compression of the core layer ($x_0(t)$). In order to analyze the response of mechanical high-pass filter at intermediate layers of an n-layer PC, $x_m(t)$ for $1 \leqslant m \leqslant n$ are also simulated and corresponding CTTFs between mth and 0th layer are denoted as $N_{pm}(s)$ (14).

The set of generalized equations defining the complex compliance ($G_i(s)$) for each layer can be written as:

$$G_0(s)=\frac{1}{H_0(s)}=\frac{X_0(s)}{F_0(s)}=\frac{M_c s^2+B_{sc} s+(K_{pc}+K_{sc})}{K_{sc}(M_c s^2+B_{sc} s+K_{pc})} \quad \text{and}$$

$$G_i(s)=\frac{1}{K_{pi}+\frac{1}{G_{si}(s)+G_{i-1}(s)}}; \quad \forall i=[1,2,\ldots,n] \quad \text{where}$$

$$G_{si}(s)=\frac{1}{M_i s^2+B_{si} s+K_{si}}; \quad \forall i=[1,2,\ldots,n] \quad (12)$$

In-between two consecutive layers force transmittance $Q_{pi}(s)$ and compression transmittance $C_{pi}(s)$) can be summarized by (13).

$$Q_{pi}(s)=\frac{F_{i-1}(s)}{F_i(s)}=\frac{1}{1+K_{pi}(G_{si}(s)+G_{i-1}(s))}; \quad \text{and}$$
$$C_{pi}(s)=\frac{X_{i-1}(s)}{X_i(s)}=\frac{G_{i-1}(s)}{G_{si}(s)+G_{i-1}(s)}; \quad \forall i=[1,2,\ldots,n] \quad (13)$$

Hence CTTF relating the compression of mth layer to core (0th) layer of PC can be written as:

$$N_{pm}(s)=\frac{X_0(s)}{X_m(s)}=\frac{G_0(s)}{G_{m-1}(s)+G_{sm}(s)}; \quad for \ \ m=1$$
$$=\left\{\prod_{i=1}^{m-1} Q_{pi}(s)\right\}\frac{G_0(s)}{G_{m-1}(s)+G_{sm}(s)}; \ \forall \ 2 \leqslant m \leqslant n \quad (14)$$

It is easy to observe in (13 and 14) that if we neglect the effect of K_{pi} (if K_{pi}=0 then $Q_{pi}(s)$=1) the model reduces to a stack of Voigt's viscoelastic model on top of the core.

The products of $Q_{pi}(s)$ in (14) contains many closely spaced poles and zeros near origin of s-plane, which generally cause instability in simulation due to the limited digital resolution in the computational tool. Therefore to avoid the instability, the compression ($x_i(t)$) of different PC layers is simulated recursively using $C_{pi}(s)$ (13). Another approach followed to avoid this instability is the approximation of the product of $Q_{pi}(s)$ form 1 to m-1 in the expression of $N_{pm}(s)$ (14), which could be $Q_{p(m-1)}(s)$ itself, as each $Q_{pi}(s)$ remains within the pass-band of $Q_{p(i-1)}(s)$ and $Q_{pi}(s)$ as well offers higher roll-off than $Q_{p(i-1)}(s)$ (referred in supplementary material). The major advantage of this approximation is the reduction of computation time as it can directly simulate $x_0(t)$ from $x_n(t)$ without simulating the mechanical signal ($x_i(t)$) at all PC layers between n and 0. This approximation makes the time-complexity of the simulation mostly independent of n for integrating this biomechanical model with neuro-physiological model of PC [31].

3 Results

3.1 PC Layer index vs. Radius

The number of lamella in PC capsule can vary from n= 20 to 70 and the peak layer thickness (Max(R_i-R_{i-1}) = Max(S_i+T_i) ~ Max(S_i)) typically reaches 10 to 15 µm [4], [10]. Therefore we have simulated 6 typical PCs with 20, 25, 30, 40, 50 and 60 lamellae and considered that all these PCs have the same peak interlamellar spacing (Max(R_i-R_{i-1}) = 12 µm) and accordingly calculated the R_i from (7) for each sample PCs (Fig. 3A).

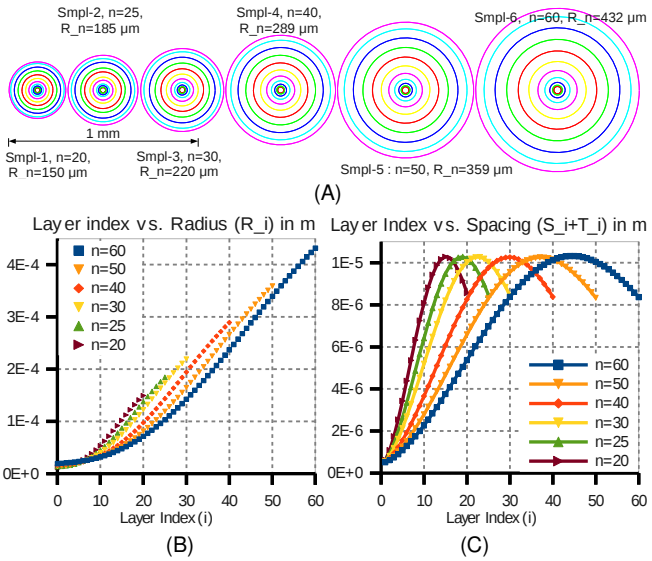

Fig. 3. A) Axial cross-section of six different size of simulated PCs; Layers are sampled at every i = 10% of n for each PC starting from inner core (i=0) till outer most layer (i=n); B) Layer index (i) vs. Radius of ith layer (R_i) and C) Layer index (i) vs. interlamellar spacing ((R_i-R_{i-1})=(S_i+T_i)) characteristics of six typical PCs considered for simulation (n = 20, 25, 30, 40, 50 and 60).

The analytical relations (6) and (7) are validated with the existing literature. The R_n and n obtained for the six simulated PC is found to be highly reasonable (Fig. 3B) compared to that obtained from Hubbard's analytical relation (1 and 2) [1], [4], especially for large value of n (>30). It is found that for initial 4 to 10 layers (growth zone), the interlamellar spacing S_i remains <1 µm which matches with [1], [6], [10], [16]. The lamellae thickness as calculated from (6), found to be restricted within 0.1 to 0.32 µm which also matches with [1].

In order to quantify the model accuracy, the analytical relation between i and R_i is compared with Hubbard's experimental result [4] which is the benchmark. However it appears that due to insufficient magnification, Hubbard

may have skipped indexing few of the layers. The smallest possible interlamellar spacing reported by Hubbard is >1 μm [4]. This contradicts the modern high magnification microscopic slides reported in [1], [6], [8], [9], [10], especially near the growth zone. Therefore Hubbard's experiment can be a benchmark with an index offset in the relation of i vs. R_i and i vs. $(S_i + T_i)$. The offset of 6, best matches the results from the proposed model, as well as the results from [3] (Fig. 4). As the experimental data from [4] explicitly indicate R_i for 20 consecutive PC layers (with offset 6, i=26) for two typical PCs (Hb_Exp_1 and Hb_Exp_2 in Fig. 4), from the six simulated PCs we have selected n=25 and 30 for comparing the results. Fig. 4 also includes the model results from Hubbard's analytical relation, denoted as Hb_Eqn. The R_i characteristic as reported in [3] is also included in Fig. 4 as Loe.

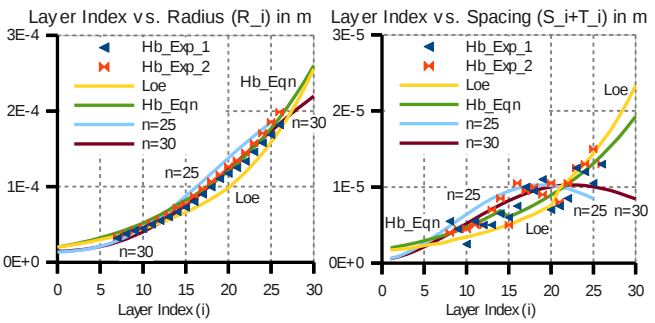

Fig. 4. A) Layer index (i) vs. Radius of ith layer (R_i) and B) Layer index (i) vs. interlamellar spacing ($(R_i\text{-}R_{i-1})$=$(S_i\text{+}T_i)$) of PCs with n=25 and n=30 layers, compared with experimental data in [4] (Hb_Exp_1 and Hb_Exp_2) and model in [3], [4] (Loe and Hb_Eqn).

The effect of abrupt change of γ of the relation (1 and 2) is clearly observable as a step in Hb_Eqn (Fig. 4B between i = 14 and 15). Similar step is observable in Loe between i = 20 and 21. However according to the microscopic slides, such step is not very distinctive in general [1], [6], [8], [9], [10] and even for the slide in [4]. On the other hand the exponential rise of Hb_Eqn (Fig. 4) indicates that it is not suitable for modeling PCs with high number of layers (n>30). Unlike Hb_Eqn, both the characteristics (n=25 and n=30 in Fig. 4B) from the proposed model indicate that final few limiting lamellae are closely spaced, which matches with [6]. In comparison to [3], the proposed model better approximates the Hubbard's experimental results for n=30 in range of 6<i≤26 (Table-1).

TABLE 1. COMPARISON OF MODEL ACCURACY

	Layer radius (R_i)		Interlamellar spacing (S_i+T_i)	
	n=30	Loe [3]	n=30	Loe [3]
	% mismatch w.r.t. layer-wise average of Hb_Exp 1 & 2			
SD over i	6.94	7.08	22.26	22.25
mean over i	-4.28	-10.26	5.23	-14.39
	Correlation Coefficient w.r.t. Hb_Exp 1 & 2			
Hb_Exp_1	0.9982	0.9932	0.7944	0.8326
Hb_Exp_2	0.9981	0.9942	0.8458	0.8761

3.2 Zonal segregation of PC lamellar structure

Table 2 indicates the zonal segregation of the perineural lamellae (Fig. 1) based on percentage of total number of lamella (n). In general the end of growth zone (GZ) is considered at 10% of n. Similarly the end of outer core (OC), outer lamellae (OL) and limiting lamellae (LL) are considered at 40%, 90% and 100% of n respectively.

TABLE 2. DIFFERENT ZONES OF PC AND RELAXATION TIME

n : $\hat{R}_n$	Layers in Zones		Zone Boundary: Layer Index (i)	R_i (μm)	% of R_n	ZW: % of R_n	CR time constant: $\tau_{25\%}$ (ms)	$\tau_{50\%}$ (ms)	$\tau_{75\%}$ (ms)
20 : 144 μm	IC	1	0% n = 0	12.6	8.4	8.4	0.659	0.714	1.024
	GZ	3	10% n = 3	16.1	10.8	2.3	0.669	0.776	3.138
	OC	6	40% n = 9	45.4	30.3	19.6	>300	>300	>300
	OL	10	90% n = 19	141.1	94.3	63.9	>300	>300	>300
	LL	1	100% n = 20	149.7	100	5.7	inf	inf	inf
25 : 178 μm	IC	1	0% n = 0	13.5	7.3	7.3	0.666	0.735	1.068
	GZ	3	10% n = 3	16.4	8.9	1.6	0.672	0.763	1.67
	OC	8	40% n = 11	52.5	28.4	19.6	>300	>300	>300
	OL	12	90% n = 23	167.1	90.5	62.1	>300	>300	>300
	LL	2	100% n = 25	184.6	100	9.5	inf	inf	inf
30 : 212 μm	IC	1	0% n = 0	14.3	6.5	6.5	0.675	0.758	1.123
	GZ	4	10% n = 4	18.5	8.4	1.9	0.685	0.811	2.128
	OC	9	40% n = 13	59.6	27.2	18.7	>300	>300	>300
	OL	15	90% n = 28	202.2	92.1	65.0	>300	>300	>300
	LL	2	100% n = 30	219.5	100	7.9	inf	inf	inf
40 : 280 μm	IC	1	0% n = 0	16.0	5.5	5.5	0.693	0.81	1.256
	GZ	5	10% n = 5	21.0	7.3	1.7	0.705	0.864	1.97
	OC	12	40% n = 17	73.9	25.5	18.3	>300	>300	>300
	OL	20	90% n = 37	263.2	91.0	65.4	>300	>300	>300
	LL	3	100% n = 40	289.3	100	9.0	inf	inf	inf
50 : 348 μm	IC	1	0% n = 0	17.7	4.9	4.9	0.714	0.869	1.415
	GZ	6	10% n = 6	23.5	6.5	1.6	0.727	0.929	2.003
	OC	15	40% n = 21	88.3	24.6	18	>300	>300	>300
	OL	25	90% n = 46	324.3	90.3	65.7	>300	>300	>300
	LL	5	100% n = 50	359.1	100	9.7	inf	inf	inf
60 : 419 μm	IC	1	0% n = 0	19.5	4.5	4.5	0.74	0.94	1.59
	GZ	7	10% n = 7	26.1	6.0	1.5	0.75	1	2.12
	OC	22	40% n = 25	103.2	23.9	17.9	>300	>300	>300
	OL	30	90% n = 55	387.8	89.8	65.9	>300	>300	>300
	LL	5	100% n = 60	431.8	100	10.2	inf	inf	inf

$\hat{R}_n$ is the approximate value of R_n used in (7); IC : Inner Core, GZ : Growth Zone; OC : Outer Core; OL : Outer Lamellae; LL : Limiting Lamellae; ZW : Zone Width; CR : Compression Relaxation; $\tau_{25\%}$, $\tau_{50\%}$ and $\tau_{75\%}$ are the time constants for 25%, 50%, 75% relaxation w.r.t. the peak compression of individual layer, against 32 μm radial step indentation at outermost layer of PC (i=n).

The 3rd column of Table 2 lists the number of lamellae present in each zone of lamellar structure for the six simulated PCs (Fig. 3A). Apart from the number of layers in different zones, 5th to 7th column of Table 2 list the variation of end-radius and zone-width based on the total number of layers present in PC (n). As shown in column 5 of Table 2, R_n as computed from (7) remains 3% to 4% higher than $\hat{R}_n$ (approximate value of R_n estimated from microscopic slides). The last 3 columns show the time constants for 25%, 50% and 75% relaxation w.r.t. peak compression of the terminal layer of each zone against 32 μm radial step indentation at outermost layer of PC (i=n).

3.3 Layerwise biomechanical properties of PC

The layerwise variation of the PC biomechanical properties is captured in three levels : 1) Elements (K_{pi}, K_{si}, B_{si} and M_i), 2) Complex compliance ($G_i(s)$) and 3) Compression transmittance ($N_{pm}(s)$). In the following section the layerwise variations of these three parameters are discussed for n=30, unless otherwise stated.

Variation of elements K_{pi}, K_{si}, B_{si} and M_i: The biomechanical properties K_{pi}, K_{si} and B_{si} (Fig. 2) as estimated using the relations (3), (4) and (5) are shown in Fig. 5. The simulation considers identical material properties for all layers (E_{li} = 1 kPa, E_{mi} = 1 Pa, U_i = 3 mPa.s, D_i = 1000 kg.m^{-3} and L = 1 mm) in order to investigate the dependency of model response over i for six simulated PCs (Fig. 3A).

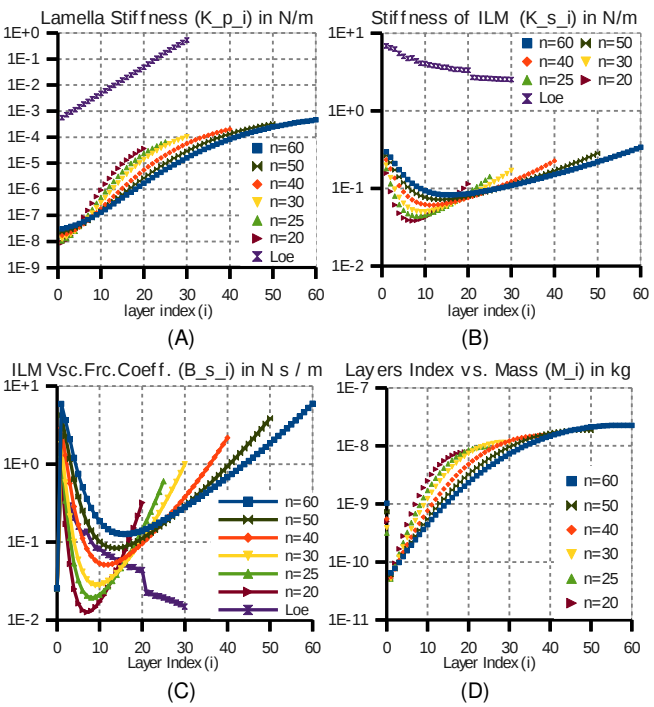

Fig. 5. A): Stiffness of lamella (parallel spring *K_p* in Fig. 2A); B): Stiffness of interlamellar matrix (serial spring *K_s* in Fig. 2A); C): Viscous frictional coefficient of interlamellar matrix (damper *B_s* in Fig. 2A); D): Mass (*M* in Fig. 2A) of each layer for PCs considered for simulation having *n*= 20, 25, 30, 40, 50 and 60 number of layers.

Validation of K_{pi}, K_{si}, B_{si} and M_i: The existing model [3] describes only a 30 layer PC based on [4] and therefore in order to validate our model, the biomechanical properties of the PC layers in [3] are also included in Fig. 5, denoted as Loe. The stiffness of lamella and interlamellar matrix from the proposed model found to be significantly lower than that of [3] (Loe in Fig. 5), which is mostly due to lower E_{li} and E_{mi}, as mentioned in section 2.4 . Similarly the nonmonotonicity of the characteristic n=30 (for K_{pi}, K_{si} and B_{si}) compared to Loe in Fig. 5 is mainly due to the nonlinearity and nonmonotonicity in the interlamellar spacing ((R_i-R_{i-1}) = (S_i+T_i)) of PC (Fig. 3C).

Variation of complex compliance ($G_i(s)$) in terms of frequency and periodic step response : The frequency response of lamellar compliance ($G_i(s)$) of a 30-layer PC (Fig. 6A). It also depicts variation of $G_i(s)$ for i = 1, 4, 10, 16, 22, 28 and 30 (two terminal and five equally spaced internal layers) which belong to different zones of PC layers (Table 2). The drop in the magnitude of $G_i(s)$ at higher frequency indicates that PC becomes stiffer as frequency increases till few kHz. On the other hand the phase difference between the compression and compressive force remains in between of -90 to -45 degree in the range of 10 to 1000 Hz for i > 15. The periodic step response (Fig. 6A-Bottom) indicates that outer lamellae creep higher than the inner lamellae due to larger interlamellar spacing and fluid content.

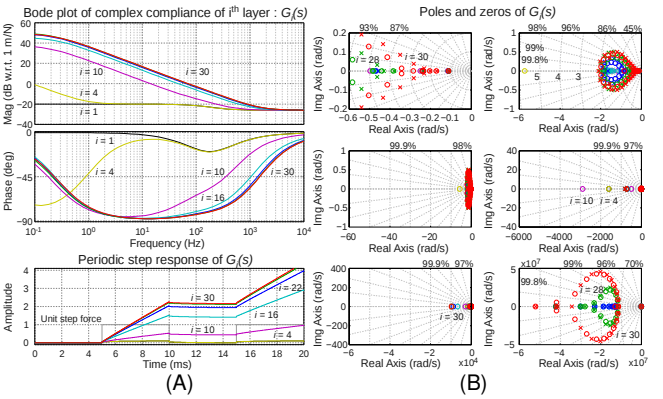

Fig. 6. Frequency response (Bode plot) (A-Top) and Periodic step response (A-Bottom) and pole-zero map (B) of complex-compliance of ith layer of a 30-layer PC ($G_i(s)$) for i = 1 (Black), 4 (Yellow), 10 (Magenta), 16 (Cyan), 22 (Blue), 28 (Green) and 30 (Red); The parameters with % indicate the damping factor corresponding to radial grids. The pole-zero maps are zoomed out from top to bottom.

Variation of complex compliance ($G_i(s)$) in terms of pole-zero map : As the poles and zeros of a transfer function governs the frequency response of a system, Fig. 6B shows pole-zero map of minimal realization of the $G_i(s)$ with order reduction below 100 by performing stable pole-zero cancellation. The pole-zero map shows under-damped poles and zeros in Hz and sub-Hz range (Fig. 6B 1,1 and 1,2). With increase of i not only the number of poles and zeros increases in PC lamellar structure but also the pseudo-elliptical pole-zero map increases its diameter. Relative placement of such high number of poles and zeros contributes to curvature (slope change) of the frequency response characteristic (Fig. 6A-Top), which in combination governs its overall shape. On the other hand larger diameter of the pole-zero map helps in preserving the effect of individual poles and zeros in frequency response preventing the larger number of pole-zero cancellation effectively. Due to consideration of mass of the PC layers, a second set of under-damped poles and zeros appears in the rage of 1 MHz to 10 MHz (Fig. 6B 3,2). It is also clear that the damping factor of the under-damped poles and zeros can only be up to 90%, causing very little overshoot in sub-Hz and MHz range. The low frequency under-damped poles make soft tissue

oscillate at Hz or sub-Hz frequency against impact loading. However the effect of MHz range under-damped poles can be observed only against ultrasonic excitation as in [32]. Therefore the effect of these second set poles and zeros are negligible in functional range of PC.

Variation of compression transmittance transfer function ($N_{pm}(s)$) in terms frequency and periodic step response : The high-pass filtering effect of PC layers is clearly visible from the Bode plot and periodic step response of CTTF $N_{pm}(s)$ for m = 1, 4, 10, 16, 22, 28 and 30 (Fig. 7A). Considering the CTTF for outermost layer (n=30 and $N_{pm}(s)$=$N_{pm}(s)$) the slope of magnitude spectrum changes significantly (~30 to ~10 dB/decade) within the functional range of PC (Few 10s of Hz to few kHz) and especially around 100 Hz. On the other hand the phase difference between the compressions of nth layer to 0th layer is found to be within 90 to 45 degree. It is clear that with the increase of the number of PC lamellae the CTTF shifts its pass-band to the right (Fig. 7A). In contrary to the creep of periodic step response of $G_i(s)$ (Fig. 6A), $N_{pm}(s)$ shows a relaxation of core (0th layer) for step compression at different (mth) layers. Time-constants of $N_{pm}(s)$ for lower m ($\leqslant$ 15) is found to be significantly higher than that of larger m (> 15), as lower value of m indicates that the step compression is applied nearer to the core (0th layer). It is also clear from Fig. 7A-Bottom that for larger m (>15), the PC inner core relaxes within 1 ms against a step compression at the PC at mth layer.

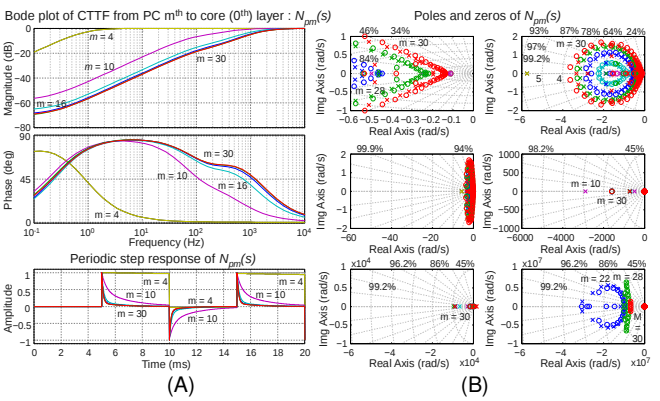

Fig. 7. Frequency response (Bode plot) (A-Top) and Periodic step response (A-Bottom) and pole-zero map (C) of CTTF from mth layer to PC core (0th) layer of a 30-layer PC ($N_{pm}(s)$) for m = 1 (Black), 4 (Yellow), 10 (Magenta), 16 (Cyan), 22 (Blue), 28 (Green) and 30 (Red); The parameters with % indicate the damping factor corresponding to radial grids. The pole-zero maps are zoomed out from top to bottom.

Variation of compression transmittance transfer function ($N_{pm}(s)$) in terms of pole-zero map : Similar to the poles and zeros of $G_i(s)$, Fig. 7B shows the pole-zero map of the CTTF $N_{pm}(s)$ which is minimal realization with order reduction below 100. In contrast to the pole zero maps of Fig. 6B, the damping factor of the under-damped poles and zeros of Fig. 7B remains as small as 50%, causing relatively higher overshoot in sub-Hz and MHz range. The presence of the over-damped largely spaced poles and zeros after angular frequency of 2π100 rad/s (Fig. 7B 2,2 and 3,1) causes slope variation in the magnitude spectrum of the CTTF especially for larger m ($10<m\leqslant n$).

3.4 Simulation of Radial compression of layers

In order to describe how the input stimulus at nth layer gets high-pass filtered at different (ith) internal layers, the compression of different layers is shown in Fig. 8A where layers ($0\leq i\leq n$) are sampled at every 10% of n=30 (periodic trapezoidal stimulus of 25 Hz with 32 µm radial compression and period to rise-time ratio = 16). The simulated compression is measured radially w.r.t. the central axis of the PC, denoted as radial compression, whereas the compression mentioned in [4] is measured w.r.t. the diameter across the central axis. In contrast to Fig. 7, Fig. 8 considers the input compressive stimulus only at outermost (nth) layer, which makes the $i\leqslant$15 characteristics relaxing faster than i>15. Similar to the trapezoidal compression Fig. 8B shows radial compression of different layers for sinusoidal stimulus (100 Hz and 1 µm) at outermost layer of PC (i=n). Fig. 8 A and B indicates that the outer core (OC) and outer lamellae (OL) gradually filters the low frequency components of the input stimulus. Therefore, with the decrease of layer index (i), the -ve phase increases in the trapezoidal stimulus and also the phase shift of compression increases in the sinusoidal stimulus. On the other hand, the limiting lamellae (LL) probably act more as a protecting cover of the capsule than taking part in high-pass filtering the stimulus. It also prevents the saturation of interlamellar space in OC and OL.

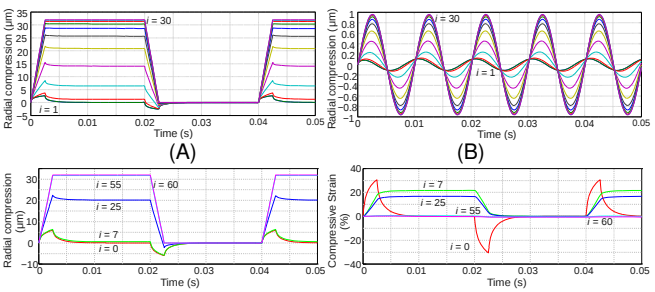

Fig. 8. Simulation of layer compression; An n=30 layer PC stimulated with A) periodic trapezoidal signal (freq = 25 Hz, radial amp= 32 µm and period to Rise-time ratio = 16) B) sinusoidal signal (freq = 100 Hz, radial amp = 1 µm) where layers are sampled at every 10% of n; C) An n=60 layer PC stimulated with periodic trapezoidal signal with same attributes as of A, where layers sampled at zone boundaries (Table 2); D) percentile inter-layer strain corresponding to C.

In order to compare the simulated result with experimental results on 800 µm diameter PC [4], we have chosen n=60 and outer diameter = 864 µm (Table 2 : Sample-6 of Fig. 3A). The motion of the layers at zone boundary (Table 2) is shown in Fig. 8C. Due to the high pass filtering of the input trapezoidal signal, the compression of the inner core (IC) and outer core (OC) appears as

pulse train. The width of the pulse obtained from this simulation with similar trapezoidal stimulus as in [4] is found to be 6 ms, which is a good match for the experimental data [4]. According to [4] in the outer core (R_i < 25% of R_n) the lamellae motions are dominated by dynamic (high frequency) component compared to its static (low frequency) component. This model also shows the similar dominance of dynamic component for the outer core lamellae (Fig. 8C). It is worth noting that though the model [3] approximately matches 6 ms pulse width, it fails to show significant attenuation of low frequency component at outer core mainly due to its limitations as mentioned in section 2.4 . Apart from the radial compression of the layer at zone boundaries, the attenuation of low frequency component is clearly visible in form of % inter-layer strain of individual layer ($(x_i(t)–x_{i-1}(t))/(R_i–R_{i-1})$.100%) as shown in Fig. 8D.

3.5 PC size vs. zone boundary & its relaxation

The size of a PC can be described in terms of either its number of layers (n) or outermost radius (R_n). Depending on size, the zone boundaries of PC layers show different relaxation patterns. The variation of PC zone boundary due to the size of PC and its biomechanical response is summarized in Table 2. Although in this model the $\hat{R}_n$ (approximate radius of outermost lamella from microscopic slides) and n can be independently selected (7), the relation of R_n vs. n becomes unique due to the constraint of maximum interlamellar spacing = 12 μm in (7), as shown in Fig. 3B & Fig. 9A row-1. With the variation of n, not only the radius of outermost layer R_n alters nonlinearly but also the boundaries of internal zones in terms of $\%R_n$ (Fig. 9A row 2 & 3). It is worth noting that for all n the zone-boundaries are defined by the fixed set of $\%n$ [0%, 10%, 40%, 90%, 100%] (Table 2).

As shown in Fig. 9B, the compression relaxation time constants of the inner core (IC) and growth zone (GZ) vary nonlinearly with the total number of lamella (n). One common feature of the characteristics of Fig. 9B is that all the relaxation time constants of IC increase monotonically with the increase of n. However such monotonicity is not maintained for the GZ lamellae. Against the step compression at outermost lamellae of PC, lamellae present after the outer core (OC) have very large compression relaxation time constant (Table 2) and hence not shown in Fig. 9B. It is worth noting that as the step compression is directly applied on the outermost lamella (m=n), the zone boundary of limiting lamellae can not relax at all, which is represented by the time constant = ∞ in Table 2. For IC the increase of time constants related to compression relaxation (Fig. 9B) is actually caused by the shift of pass-band of the $N_{pn}(s)$ with the increase of n. Such shift of the pass band has a similarity with the reduction of the cutoff of the lamellar high-pass filter as layer index (m) increases (Fig. 7). The 3 dB cutoff of $N_{pn}(s)$ for below 40-layer PC is found to be in the range of 1 to 2 kHz and it goes below 1 kHz if the number of layers is increased further (Sample-5 and sample-6 in Fig. 3A).

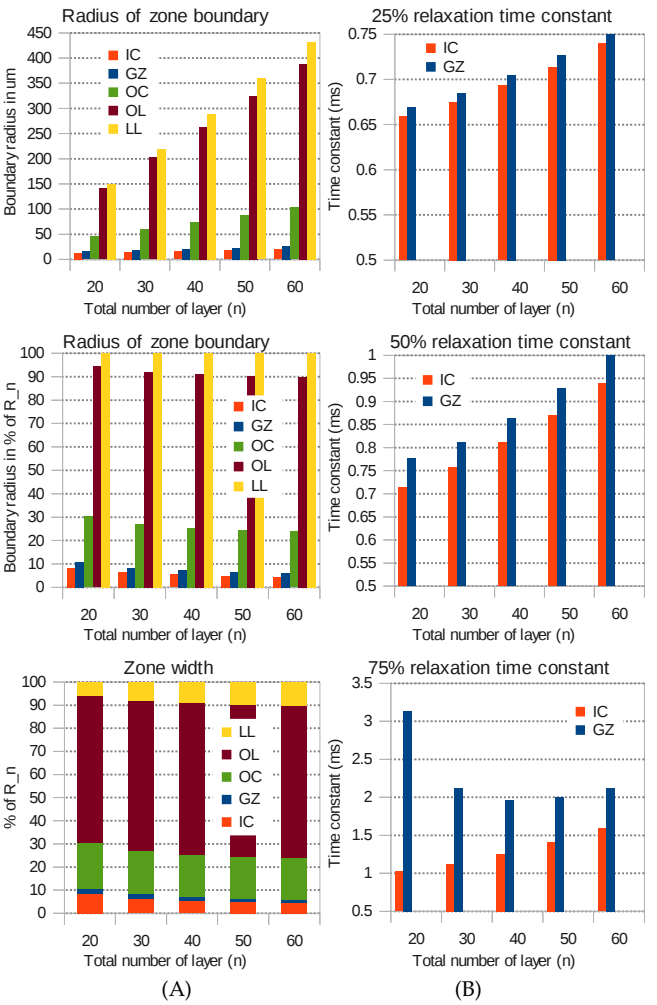

Fig. 9. A) Variation of zone boundary and zone width depending on the number of layers (n). B) Variation of inner core and growth zone relaxation time-constants due to step compression at outermost layer of PC; IC : inner core, GZ : growth zone, OC : outer core, OL : outer lamellae, LL : limiting lamellae (Fig. 1 and Table 2).

4 Discussion

PC size and lamella distribution: One of the major contributions of this work is the formulation of better analytical relation between radius of PC outermost layer (R_n) and number of layer (n). The size and lamella distribution of PC are empirically estimated from the recently published high magnification microscopic slides and description of lamellar structure of PC in [1], [6], [8], [9], [10] along with the low magnification slides and description in [1], [4]. This in turn shows that Hubbard's analytical relation [1], [4] holds good only for small PCs or PCs with augmented outer lamellae. The proposed model describes more generalized relation (7) between radius of different layers (R_i) and layer index (i) considering the inner core as the 0^{th} layer. Therefore it can also formulate systematic categorization of different zones of the PC

capsule with the indication of range of radius and the number of layer in different zones. The analytical relation for a 30 layer PC is quantitatively compared with the data available from [3], [4] and found that the proposed relation is a better fit even for small PCs (n= 30 in Fig. 4 and Table 1). Along with the 30 layer PC, using the same analytical relation six different size of PCs are simulated (R_n = 150 to 432 μm). Though these six PCs (Fig. 3 and Table 2) contain different numbers of layers (n = 20, 25, 30, 40, 50 and 60) and radii, they have a common maximum interlamellar spacing 12 μm (10-15 μm) which appears to be more generalizable property for different PCs described in [1], [4], [6], [8], [10], as shown in Fig. 3. This model also captures 3 to 4% reduction in R_n to $\hat{R}_n$ using (7) when PC layers are punctured [1], [2].

Biomechanical characteristics of PC lamellar structure : Another contribution of this model is the formulation of recursive transfer-functions related to complex-compliance $G_i(s)$ and compression transmittance (CTTF) $N_{pm}(s)$ of different layers of PC. The frequency response of $G_i(s)$ indicates that PC outermost layer can be few 1000 times stiffer in the kHz range compared to the sub-Hz range (6). Similarly the frequency response and periodic step response of CTTF $N_{pm}(s)$ clearly describes the high-pass filtering effect of PC lamellar structure. It is also observed that with the increase of size and layer number, the cutoff of the lamellar high-pass filter drops which makes the pass-band wider and PC more sensitive towards relatively low frequency stimulus (Fig. 7 and Fig. 9B). Such lowering of the cutoff probably indicates the reason why the young people are more sensitive to high frequency vibration than the older [33], as it is well known that PC increases its size and number of layers with the age [5], [34]. However one advantage of larger PC as predicted from this model is that they have higher detectability to a random stimulus as they have wider pass band. This actually helps in compensating the extra attenuation of stimulus for the subcutaneous PCs as they are typically found to be larger in size than the PCs in dermis [1], [34], [35].

Material properties of PC : The response of this model is significantly sensitive to the material properties of PC used for calculating the system parameter K_{pi}, K_{si} and B_{si} of the biomechanical model. For the simulation reasonable range of elastic modulus of lamella (E_L) and viscosity of interlamellar matrix (U) is found to be 1 to 2 kPa and 1.5 to 7 mPa.s respectively. Apart from B_{si}, as obtained from the chosen viscosity (5), the viscous frictional coefficient of inner core (B_{s0}=B_{sc} of Fig. 2) is another sensitive parameter, considered as 0.0255 N.s.m^{-1}, which is 5 to 10 times lower than the minimum of B_{si} for $0<i\leq n$. It controls the peak % strain at the inner core (Fig. 8D). In the chosen PC model, outermost layer can undergo compression beyond 20% of R_n without saturation of interlamellar space in capsule or excessive compression of inner core.

Order of the model : In the proposed model the PC inner core is considered as Voigt's model with a serial spring resulting in a 1st order bi-proper transfer function if mass is neglected and becomes 2nd order bi-proper if mass-effect is included. This can also be approximated as 1st or 2nd order bi-proper version of Kelvin's model. However with alteration of mass position in Kelvin's model as shown in [28] the transfer function becomes 3rd order strictly-proper (8), which has inherent limitation of creating high-frequency jitters in transits while attempting to simulate low-frequency creep simultaneously.

Effect of mass : From this simulation it is found that the effect of mass is negligible in the functional range of PC (few 10s of Hz to few kHz). However the effect of mass is clearly observable in terms of under-damped poles and zeros in the frequency range >1 MHz (Fig. 6 and Fig. 7 pole-zero map 3,2). If PC core is modeled as 3rd order transfer-function similar to (8) the effect of mass is observable even below 1 MHz. In comparison to mass, the response of this proposed model is found to be more sensitive on the viscosity and elastic modulus of the interlamellar matrix as well as that of the lamella.

Core relaxation and validation : The developed model is validated with the experimental data in [4] considered as benchmark. When the outermost lamella of PC is stimulated with a step indentation the inner core relaxes within 1 ms for small and medium size PC (n<40 in Fig. 3A). However as the PC selected by Hubbard in his experiment is larger in diameter (800 μm) it creates ~6 ms pulse of indentation against trapezoidal stimulus [4], which matches with this simulation result (Fig. 8C). However against the step indentation, even such large PC shows 90% relaxation of inner core within 2 ms. As the PC inner core follows higher order relaxation characteristics, Table 2 summarizes them in terms of 25%, 50% and 75% relaxation time-constants for all six PCs selected (Fig. 3A).

Improvement over existing models : The proposed model is significantly different from several simple biomechanical models which approximate PC lamellar filter as a linear combination of differentiators of different order [13], [18], [36] for directly matching the mechanical stimulus to neural response. The proposed model is not only capable of showing the differentiation process, but also the zone where it occurs (around outer core). The limiting lamellae and the outer lamellae mostly drifts instead of differentiating the trapezoidal stimulus, which in turn helps in stabilizing the outer core and preventing the saturation of interlamellar space. Therefore interlamellar spacing plays a significant role in defining the frequency response of this biomechanical filter. Unlike the existing models, the proposed model uses material properties of PC such as the viscosity of the interlamellar matrix and the viscous frictional coefficient of the inner core which are important in governing the response of the lamellar filter. Although this model assumes homogenous material properties due to the lack of explicit data available in

literature, it has provision for incorporating inter-layer heterogeneity. The layerwise inhomogeneity can also be assessed by the reverse estimation of the model parameters from the experimental data as in [4].

Computational accuracy in simulation : Apart from a detailed model, this paper describes methods for achieving better computational accuracy in the simulation of biomechanical response of PC. One major challenge in this simulation is the consideration of the mass. The pole-zero map of the complex-compliance ($G_i(s)$) and the CTTF ($N_{pm}(s)$) indicates the poles and zeros contributed by mass belongs to MHz range (Fig. 6 and 7) and therefore it can be safely neglected in the functional range of PC (few 10s of Hz to few kHz). This simplification also reduces the order of the transfer functions $G_i(s)$, $Q_i(s)$ and $N_{pm}(s)$, which helps in simulating the compression signal for PCs with layer number n>30. If the effect of mass is considered, the order of the $N_{pm}(s)$ crosses 500 even for n=30 in a non-minimal realization of the transfer-functions. Therefore to restrict the order of the transfer functions below 100 in their minimal realization, the tolerance for pole-zero cancellation is selected in-between $eps^{0.5}$ to $eps^{0.1}$, where eps is the machine epsilon (2.2204e-16). This introduces little inaccuracy in the simulation in frequency only below 0.1 Hz. However a higher tolerance for pole-zero cancellation can cause significant inaccuracy in even below 1 Hz and hence avoided in this simulation. The requirement of the minimal realization is observable from the pole-zero map of the transfer functions (Fig. 6 and 7). More than the high frequency under-damped poles and zeros, the sub-Hz under-damped poles and zeros make the model stability vulnerable, as computational error accumulates during simulation and few of the poles may gradually shift to the right half of s-plane. However the model stability and computational accuracy is improved by neglecting mass-effect and reducing the model order with minimal realization of the transfer functions. From Fig. 6 it is clear that the damping factor of the under-damped poles and zeros in complex compliance can be as low as 90% causing very little overshoot in sub-Hz and MHz range. It is interesting to note that in the functional range of PC (few 10s of Hz to few kHz) the poles and zeros of $N_{pm}(s)$ remains over-damped, whereas the under-damped poles and zeros in sub-Hz range can have damping factor as low as 50%. From the frequency response and pole-zero map of $N_{pm}(s)$ (Fig. 7) it is fair to conclude that the lower cutoff of $N_{sp}(s)$ remains in the order of 1 kHz and the band-width extends beyond 10 kHz which helps in maintaining vibrotactile sensitivity beyond 1 kHz [37], [38], [39].

Limitations of the model : This simulation considers linear biomechanical model as the stimulus amplitude typically remains below 100 μm in the functional frequency range of PC causing less than 20% strain in any layer. Therefore considering [40], [41] it appears that for such small compression, PC biomechanics would remain significantly linear. However for larger stimulus it is found that lamellae of two consecutive layers may touch each other causing higher degree of nonlinearity, which may be addressed by considering piece-wise linear biomechanical properties for different range of stimulus. It is worth noting that the direct simulation of inner core compression using the approximated $N_{pm}(s)$ as described in section 2.5 (14), introduces <2% error compared to iterative layer-wise simulation of the inner core compression. Though this model can show higher attenuation of the static component in outer core (OC) compression compared to [3] which matches well with the experimental result of [4], the attenuation of static component of inner and outer lamellae (OL) remains lower in the response of proposed model compared to [4]. One of the major reasons of this mismatch is probably due to the interlamellar inhomogeneity of the material properties as well as the approximation of PC as concentric cylinders. Although the model has provision to account for the depth of PC in skin column, in this paper interaction between skin and PC are not detailed, which is out of scope of this paper.

Summary : This paper not only describes a layered analytical model of PC lamellar structure but also generalizes the model over various sizes of the PC. It also summarizes various details of PC lamellar structure in recent literature in order to develop this model. The simulated response of this model for a 30 layer PC matches well with the experimental result in [4]. Therefore this model can be considered as a major improvement over of the existing simple biomechanical models as well as the detailed model from [3]. Although the main objective of this paper is to analyze the effect of size variability of PC on only the relaxation response, it can also be extended to study this effect on the well-known U-shaped neural response of PC [30], [31]. In spite of its few limitations, this model has potential in simulating a network of various PCs for investigating the mechanism of enhancing the high-frequency vibration perception through skin. This model can also be adopted for simulating and analyzing the physiology of other corpuscular lamellar mechanoreceptor like Herbst's corpuscle [42], [43] typically found in non-mammalian species like birds.

REFERENCES

[1] J. Bell et al., "The structure and function of pacinian corpuscles: A review," *Prog. Neurobiol.*, vol. 42, no. 1, pp. 79–128, Jan. 1994.

[2] D. C. Pease and T. A. Quilliam, "Electron Microscopy of the Pacinian Corpuscle," *J. Biophys. Biochem. Cytol.*, vol. 3, no. 3, pp. pp. 331–342, 1957.

[3] W. R. Loewenstein and R. Skalak, "Mechanical transmission in a Pacinian corpuscle. An analysis and a theory," *J. Physiol.*, vol. 182, no. 2, pp. 346–378, Jan. 1966.

[4] S. J. Hubbard, "A study of rapid mechanical events in a mechanoreceptor," *J. Physiol.*, vol. 141, no. 2, pp. 198–218, 1958.

[5] N. Cauna and G. Mannan, "The structure of human digital pacinian corpuscles (corpus cula lamellosa) and its functional significance.," *J. Anat.*, vol. 92, no. 1, pp. 1–20.4, 1958.

[6] P. Dubovy and J. Bednarova, "The extracellular matrix of rat Pacinian corpuscles: an analysis of its fine structure," *J. Anat. Embryol.*, vol. 200, pp. 615–623, May 1999.

[7] B. Munger et al., "A re-evaluation of the cytology of cat Pacinian corpuscles," *Cell Tissue Res.*, vol. 253, no. 1, pp. 83–93, 1988.
[8] L. Pawson et al., "Immunocytochemical identification of proteins within the Pacinian corpuscle.," *Somatosens. Mot. Res.*, vol. 17, no. 2, pp. 159 – 170, 2000.
[9] L. Pawson and S. J. Bolanowski, "Voltage-gated sodium channels are present on both the neural and capsular structures of Pacinian corpuscles," *Somatosens. Mot. Res.*, vol. 19, no. 3, pp. 231–237, 2002.
[10] K. Sames et al., "Lectin and Proteoglycan Histochemistry of Feline Pacinian Corpuscles," *J. Histochem. Cytochem.*, vol. 49, no. 1, pp. 19–28, Jan. 2001.
[11] H. Irie et al., "Painful heterotopic pacinian corpuscle in the hand: a report of three cases," *Hand Surg.*, vol. 16, no. 01, pp. 81–85, 2011.
[12] F. Vaes and L. D. Smet, "A rare cause of digital pain: the subepineural Pacinian corpuscle," *Eur. J. Plast. Surg.*, vol. 26, no. 7, pp. 370–372, 2003.
[13] F. Grandori and A. Pedotti, "Theoretical Analysis of Mechano-to-Neural Transduction in Pacinian Corpuscle," *IEEE T. Biomed. Eng.*, vol. BME-27, no. 10, pp. 559–565, Oct. 1980.
[14] M. H. Holmes and J. Bell, "A Model of a Sensory Mechanoreceptor Derived From Homogenization," *SIAM J. Appl. Math.*, vol. 50, no. 1, pp. 147–166, 1990.
[15] L. J. Drew et al., "Touch," in *Mechanosensitive Ion Channels, Part B*, vol. 59, O. P. Hamill, Ed. Academic Press, 2007, pp. 425 – 465.
[16] L. Malinovský et al., "The capsule structure of Pacinian corpuscles from the cat mesentery.," *Z Mikrosk Anat. Forsch.*, vol. 104, no. 2, pp. 193–201, 1990.
[17] B. L. Munger and C. Ide, "The enigma of sensitivity in Pacinian corpuscles: a critical review and hypothesis of mechano-electric transduction," *Neurosci. Res.*, vol. 5, no. 1, pp. 1–15, Oct. 1987.
[18] S. Bensmaia et al., "Conveying tactile feedback using a model of mechanotransduction," in *BioCAS. IEEE*, 2008, pp. 137–140.
[19] J. Bell and M. H. Holmes, "A note on modeling mechano-chemical transduction with an application to a skin receptor," *J. Math. Biol.*, vol. 32, no. 3, pp. 275–285, 1994.
[20] L. Yang, "Mechanical properties of collagen fibrils and elastic fibers explored by AFM," University of Twente, Enschede, 2008.
[21] Frederick H. Silver et al., "Viscoelastic properties of young and old human dermis: A proposed molecular mechanism for elastic energy storage in collagen and elastin," *J. Appl. Polym. Sci.*, vol. 86, no. 8, pp. 1978–1985, Jan. 2002.
[22] K. Gelse et al., "Collagens-structure, function, and biosynthesis," *J. Adv. Drug Deliv. Rev.*, vol. 55, pp. 1531–1546, Aug. 2003.
[23] M. P. Jacob, "Extracellular matrix remodeling and matrix metalloproteinases in the vascular wall during aging and in pathological conditions," *J. Biomedicine & Pharmacotherapy*, vol. 57, no. 5/6, pp. 195–202, 2003.
[24] G. A. Holzapfel, *Collagen: Structure and Mechanics*. Heidelberg, Germany: Springer, 2008.
[25] W. Xu et al., "Cell Stiffness Is a Biomarker of the Metastatic Potential of Ovarian Cancer Cells," *PLoS ONE*, vol. e46609, 2012.
[26] E. A. G. Peeters et al., "Viscoelastic Properties of Single Attached Cells Under Compression," *J. Biomech. Eng.*, vol. 127, no. 2, pp. 237–243, Sep. 2004.
[27] S. Newman et al., "Viscosity and elasticity during collagen assembly in vitro: Relevance to matrix-driven translocation," *Biopolymers*, vol. 41, no. 3, pp. 337–347, 1997.
[28] A. Biswas et al., "A Biomechanical Model of Pacinian Corpuscle & Skin," in *Biomedical Science and Engineering Conference (BSEC)*, ORNL, Oak Ridge, TN, USA, 2013, pp. 1–4.
[29] B. Rydqvist et al., "Visco-elastic properties of the rapidly adapting stretch receptor muscle of the crayfish," *Acta. Physiol. Scand.*, vol. 150, no. 2, pp. 151–159, 1994.
[30] A. Biswas et al., "Nonlinear Two Stage Mechanotransduction Model and Neural Response of Pacinian Corpuscle," in *Biomedical Science and Engineering Conference (BSEC)*, ORNL, Oak Ridge, TN, USA, 2014, pp. 1–4.
[31] A. Biswas et al., "Vibrotactile Sensitivity Threshold: Nonlinear Stochastic Mechanotransduction Model of Pacinian Corpuscle," *IEEE Trans. Haptics*, vol. Submitted for publication, 2014.
[32] X. Yang and C. C. Church, "A simple viscoelastic model for soft tissues the frequency range 6-20 MHz," *IEEE Trans. Ultrason., Ferroelectr., Freq. Control*, vol. 53, no. 8, pp. 1404–1411, 2006.
[33] C. Wells et al., "Regional variation and changes with ageing in vibrotactile sensitivity in the human footsole.," *J. Gerontol. A Biol, Sci. Med. Sci.*, vol. 58, no. 8, pp. 680–686, Aug. 2003.
[34] K Kumamoto et al., "Distribution of pacinian corpuscles in the hand of the monkey, Macaca fuscata," *J. Anat.*, vol. 183, pp. 149–154, 1993.
[35] Z. Halata, "The ultrastructure of the sensory nerve endings in the articular capsule of the knee joint of the domestic cat (Ruffini corpuscles and Pacinian corpuscles)," *J. Anat.*, vol. 124, no. 3, pp. 717–729, 1977.
[36] R. G. Dong et al., "Estimation of the biodynamic responses distributed at fingers and palm based on the total response of the hand–arm system," *Int. J. Ind. Ergonom.*, vol. 40, no. 4, pp. 425–436, 2010.
[37] L. D. Goodfellow, "Vibratory sensitivity: its present status," *Psychol. Bull.*, vol. 31, no. 8, pp. 560–571, Oct. 1934.
[38] V. O. Knudsen, "'Hearing' with the Sense of Touch," *J. Gen. Psychol.*, vol. 1, no. 2, pp. 320–352, 1928.
[39] L. Wyse et al., "Perception of vibrotactile stimuli above 1kHz by the hearing-impaired," presented at the 12th Internation Conference on New Interfaces for Musical Expression, University of Michigan, Ann Arbor, Michigan, USA, 2012.
[40] L. Barbé et al., "Needle insertions modeling: Identifiability and limitations," *Biomedical Signal Processing and Control*, vol. 2, no. 3, pp. 191 – 198, 2007.
[41] R. J. Gulati and M. A. Srinivasan, "Determination of Mechanical Properties of human Fingerpad in Vivo Using a Tactile Stimulator," Touch Lab, MIT, Massachusetts, USA, M.S. Thesis, 1997.
[42] K.-M. Gottschaldt et al., "Thermosensitivity and its possible fine-structural basis in mechanoreceptors in the beak skin of geese," *J. Comp Neurol.*, vol. 205, no. 3, pp. 219–245, 1982.
[43] P. H. J. Nafstad and A. E. Andersen, "Ultrastructural investigation on the innervation of the Herbst corpuscle," *Z. Zellforsch. Mik. Ana.*, vol. 103, no. 1, pp. 109–114, 1970.

Abhijit Biswas got his B.Tech. in Electronics and Instrumentation from University of Kalyani and M.E. in Biomedical Engineering from Jadavpur University, Kolkata in 2006 and 2008 respectively. He worked in Robhatah Robotic Solutions Pvt. Ltd., a spin-off company of National University of Singapore, as Sr. R&D Engineer for two years and joined Touch Lab, IIT Madras as a research scholar.

M. Manivannan holds PhD and ME degrees from the Indian Institute of Science, Bangalore. He received post-doctoral training in Haptics at the MIT, Cambridge. Before MIT, he received another post-doctoral training in CAD standards and Sensors Network at the National Institute of Standards and Technology, Maryland. He served as a chief software architect of Yantric Inc. before joining IIT Madras.

Mandayam A. Srinivasan is the founder and director of the MIT Touch Lab and Senior Research Scientist at MIT's Department of Mechanical Engineering and the Research Laboratory of Electronics. He is also Professor of Haptics at the Department of Computer Science, UCL. His research interests include haptic computation, cognition, and communication in humans and machines, particularly to enhance human–machine interactions in VR and teleoperation systems. He has a PhD from the Department of Mechanical Engineering at Yale University.